Anatomia, Histologia, Embryologia

WILEY

ORIGINAL ARTICLE OPEN ACCESS

Measuring Equine Hooves in Radiographs and Computed Tomography Images Reveals Unexpected Size Differences

Lina Sellke[1] | Eberhard Ludewig[2] | Stephan Handschuh[3] | Kirsti Witter[1]

[1]Department of Biological Sciences and Pathobiology, Unit of Morphology, University of Veterinary Medicine Vienna, Vienna, Austria | [2]Diagnostic Imaging – Clinical Center of Small Animals, Clinical Department for Small Animals and Horses, University of Veterinary Medicine, Vienna, Vienna, Austria | [3]VetCore Facility for Research/Imaging Unit, University of Veterinary Medicine, Vienna, Vienna, Austria

Correspondence: Kirsti Witter (kirsti.witter@vetmeduni.ac.at)

Received: 2 September 2025 | **Revised:** 26 November 2025 | **Accepted:** 1 December 2025

Keywords: dimensional measurement accuracy | distance measurements | horse | mathematical correction | radiographic magnification | volume rendering

ABSTRACT

In a previous study on hoof biometry, we found that mathematical correction of measuring results from radiographs did not lead to complete correspondence to computed tomography (CT) results. The present study investigates this finding by comparing 13 measures of six cadaveric equine digits collected with the following workflows: radiographs with 1 and 2 m focus-object distance (FOD) (Xray 1 m/2 m), computed tomography images in planes defined based on anatomical landmarks (CTw), simulated radiographs based on the tomography dataset (virtual 120-mm slabs, Xray Sim) and measurements based on slices and projections aided by three-dimensional reconstruction models of hooves and bones based on the tomography data set (AMIRA). Furthermore, Xray 1 m/2 m values were mathematically corrected using factors calculated for each hoof (Xray 1 m/2 m corr). Results of all methods correlated, but absolute values showed differences. Xray 1 m/2 m values were systematically higher, Xray Sim and AMIRA values were lower than CTw values. Increasing FOD and mathematical correction of Xray values led to approximation to CTw values. Among measures producing unexpected results and large differences between methods were palmar process height, medial and lateral (but not dorsal) hoof wall thickness, dorsal hoof wall length, weight-bearing length and heel/toe to plumbline. Explanations might be primarily different definitions of landmarks in different methods, but also contrast settings for displaying both bone and soft tissue contours. Therefore, when comparing the measuring results collected using different methods, it is advisable to analyse relative rather than absolute values.

1 | Introduction

The size of structures in radiographs representing perspective projection images is known to be larger than the actual size of these structures (Goulet et al. 2015; Kumar et al. 2007; Nilsson et al. 2004; Stevens 1989; Tjernström et al. 1996) (Figure 1). If required, the measuring results can be mathematically corrected based on the intercept theorem (Buckle et al. 2013; Kumar et al. 2007; Wechselberg and Wessely 1973). Measuring results from computed tomography (CT) images usually reflect the actual distances with high accuracy (Gaspoz et al. 2015; Vasconcellos et al. 2015). Observed differences between fan-beam or cone beam CT measuring results and dimensions measured in real objects (bones, body parts) are discussed, especially in fields where precise measuring is of great importance, such as in implantology and material science (Fatemitabar and Nikgoo 2010; Kruth et al. 2011; Mozzo et al. 1998).

In a recent study comparing different methods of equine hoof biometry, we found that measuring results collected from radiographs were systematically higher than those taken from CT images as one would expect (Sellke et al. 2023). Surprisingly, even after correction of the values for linear measures using the intercept theorem (Stevens 1989), a smaller but still existent difference remained between radiographs and CT images for many of the measures. The first attempt to get closer to the presumably correct measured CT values (CT workflow—CTw; see Section 2) was to take the radiographs with a 2 m focus-object distance (FOD) instead of 1 m. This reduced the differences but still did not fully explain the divergence of data.

The aim of the study was to analyse this problem in greater detail. Hoof measures collected using various imaging techniques and methods of data acquisition were compared. Differences are discussed and attempts are made to identify possible factors generating systematic differences between measures collected by the different workflows.

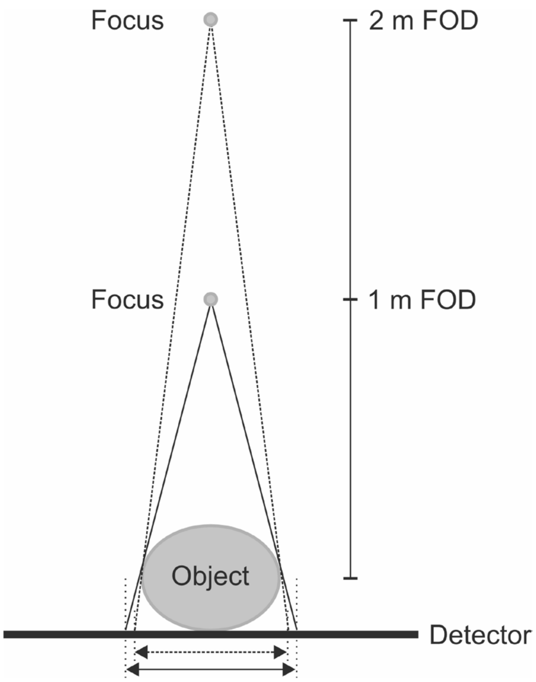

FIGURE 1 | Projection of objects in radiographs depending on focus-object-distance (FOD). Both projections are larger than the dimensions of object, but the projection with 1-m FOD is larger than that with 2-m FOD.

2 | Material and Methods

Six cadaveric front limbs of adult horses that died or were euthanized for health reasons unrelated to this study at the University for Veterinary Medicine in Vienna were used. The study was carried out in accordance with the university's regulations on the use of cadaveric material.

Size and conformation of the equine hooves and limbs differed, but there were no obvious pathologies preventing the planned measurements. The limbs were stored at −20°C and thawed before imaging.

The limbs were subjected to CT and digital radiography. A set of hoof measures that are standardly assessed for scientific and medical reasons (Sellke et al. 2020) was collected for this study using seven different workflows (Table 1). In total, 13 hoof measures were taken (Table 2, Figure 2). Except for the dorsal hoof wall length, all measures could be recorded with all approaches.

All measurements were performed by a single observer (LS). Intraobserver variability was assessed in a preliminary study for CTw, Xray 1 m and AMIRA and considered negligible (Intraclass Correlation Coefficient > 0.99). Corresponding measuring results of the same hoof collected with the different methods were compared.

2.1 | Image Acquisition

To avoid marker-based artefacts, CT was performed before the radiographic examination. A 16-slice medical helical CT scanner (Somatom Emotion, Siemens Healthcare, Erlangen, Germany) was used. For hygienic reasons, the limbs remained wrapped in

TABLE 1 | Abbreviations and short descriptions of the seven analysed measuring workflows. For details see text.

Abbreviation	Workflow
Xray 1 m	Radiography in lateromedial and dorsopalmar projection using radioopaque markers, focus-object-distance 1 m, image processing and measuring using JiveX
Xray 2 m	As above, focus-object distance 2 m
Xray 1 m corr	Mathematical correction of Xray 1 m values to exclude projection magnification by a factor calculated individually for each hoof (Figure 3)
Xray 2 m corr	As above, for Xray 2 m values
CTw	Computed tomography images reformatted in planes based on anatomical landmarks and measuring using JiveX
Xray Sim	Computed tomography, reformatting into 120-mm thick slabs in average intensity projection mode to simulate radiographs in lateromedial and dorsopalmar projection, measuring as described for Xray 1 m; image processing and measuring using JiveX
AMIRA	Measurements from CT data (virtual CT slices and maximum intensity projections) that were manually oriented based on anatomical landmarks aided by 3D reconstructed models of the bones and the outer surface of the hoof

TABLE 2 | The 13 hoof measures analysed in this study, including their definition. For illustrations see Figure 2 and Sellke et al. (2020).

Measure (number)	Definition
Weight-bearing length (1)	Length of *Facies contactus* of *Facies solearis*
Hoof width (2)	Linear distance between the widest part of *Pars lateralis/medialis*
Dorsal hoof wall length (3)	Linear distance from the most dorsoproximal point of *Pars dorsalis* and along the hoof wall to the ground line
Dorsal hoof wall thickness proximal (4)/distal (5)	Linear distance between the outermost extent of *Pars dorsalis* of the hoof and the dorsal cortex of *Phalanx distalis*, measured perpendicular to *Pars dorsalis*
Lateral (6)/medial (7) palmar process height	Vertical distance between *Proc. palmaris lateralis/medialis* and the ground line
Thickness of the sole (8)	Vertical distance between the tip of *Phalanx distalis* and the ground
Lateral (9)/medial (10) hoof wall thickness	Shortest linear distance between the outer surface of *Pars lateralis/medialis* of the hoof capsule and *Phalanx distalis*, measured perpendicular to *Pars lateralis/medialis*
Heel to plumbline (11)	Linear distance between the most caudal part of *Facies contactus* of *Facies solearis* and the plumb line through the centre of rotation of *Caput phalangis mediae*
Toe to plumbline (12)	Linear distance between the most dorsal part of *Facies contactus* of *Facies solearis* and the plumb line through the centre of rotation of *Caput phalangis mediae*
Distal interphalangeal joint-to-ground distance (13)	Shortest vertical distance between *Facies articularis* of *Phalanx distalis* and the ground

a plastic bag during scanning. No special positioning devices were used. Transverse scans along the limb axis were acquired at 130 kVp, 200 mAs, a slice thickness of 0.5 mm, a rotation time of 1 s and a pitch of 0.8. The field of view was approximately $160 \times 160\,mm^2$ with a scan matrix size of 512×512 pixels. Depending on specimen size, the resulting voxel size ranged from $0.24 \times 0.24 \times 0.5$ mm to $0.33 \times 0.33 \times 0.5$ mm in the *x*-, *y*- and *z*-axis, respectively.

For radiography, the limbs were mounted vertically on a stand to mimic the position of a loaded limb (but not the pressure exerted by the weight of a living horse). Radiopaque markers were placed on the specimens to identify relevant landmarks as described below. The radiographs were acquired using a stationary X-ray machine designed for horse examinations (Super 100, PHILIPS Healthcare, Hamburg, Germany). The images were recorded with a digital flat panel detector (FDR D-EVO II C24, Fujifilm, Tokyo, Japan). X-ray source settings of 60 kVp and 10 mAs resulted in values of the exposure indicator in the range of dose of $S = 400 \pm 40$. Other exposure parameters, focal spot size of $1.2 \times 1.2\,mm^2$, total filtration of 2.0 mm, and no use of an anti-scatter grid, were kept constant for all radiographs.

Two sets of radiographs were taken from each digit: (i) with a focus-object distance of 1 m (standard) in lateromedial and dorsopalmar projection, and (ii) with a 2-m focus-object distance also in both projections. For the lateromedial projections, the central beam was tilted about 1°–2° and a barium sulphate (Ba_2SO_4) paste marking was added at the most dorsal point of the coronary band and at the coronary band of the heel closer to the detector. Furthermore, a metal bar was fixed at the tip of the frog. For the radiographs in dorsopalmar projection, the existing markers were left in place and additional Ba_2SO_4 paste was added laterally and medially at the widest part of the coronary band.

As a part of quality assurance measures of the institution, the CT scanner and the detector system for X-ray images are checked and calibrated monthly according to established protocols. Tests are carried out using phantoms, including those for analysing spatial resolution and geometric properties.

2.2 | Image Presentation and Measurements

The radiographs and computed tomography files were exported in DICOM format and processed and analysed using a dedicated workstation equipped with the medical DICOM viewer (JiveX, VISUS Health IT GmbH, Bochum, Germany). The transverse computed tomography data sets were reformatted into image planes usable for measurement based on anatomical landmarks (multiplanar reconstruction of 3-mm slabs in average intensity projection; for details see Sellke et al. 2023). A bone window setting (window width 3100 HU, window level + 500 HU) was used for measures including at least one bone landmark, a soft tissue window setting (window width 280 HU, window level + 50 HU) for measures including only soft tissue landmarks.

To simulate conventional radiographs, average intensity projections of 120-mm thick slabs were generated from the computed tomography dataset in lateromedial and dorsopalmar projections.

Measurements in radiographs, simulated radiographs and CT images were performed using the distance measurement tool of the JiveX software. For optimal visualisation, brightness and contrast of the radiographs were adjusted to the observer's discretion. Landmarks were defined as described by Sellke et al. (2020) using the Ba_2SO_4 and metal markers as landmarks when

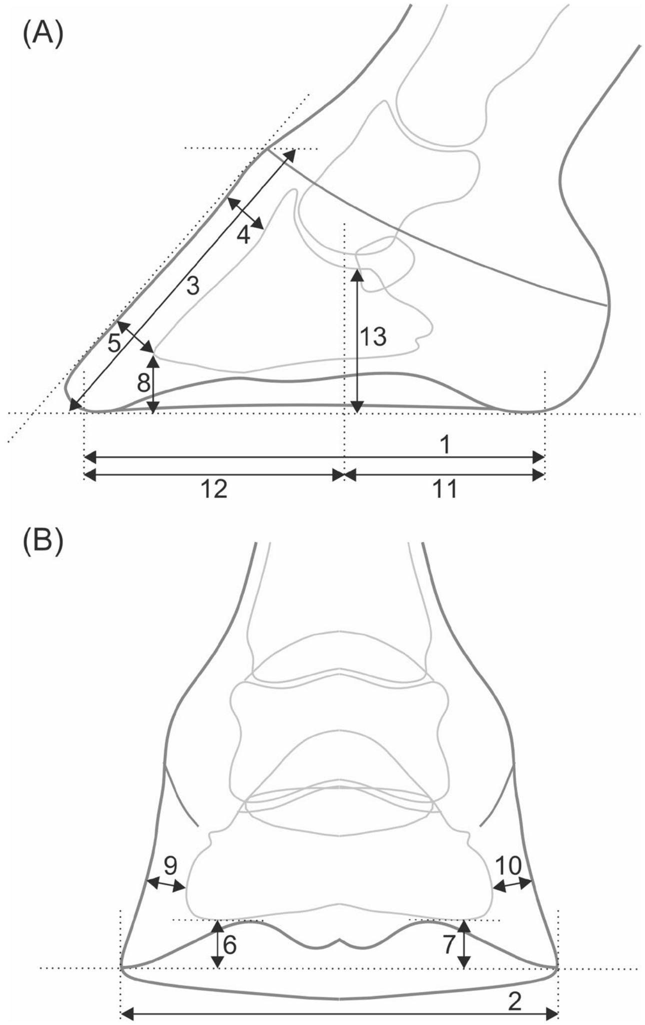

FIGURE 2 | Schematic illustration of the hoof measures used in this study. (A) Lateral view; (B) dorsal view. Light grey lines represent significant bone contours, dark grey lines soft tissue contours. Weight-bearing length (1), hoof width (2), dorsal hoof wall length (3), dorsal hoof wall thickness proximal (4)/distal (5), lateral (6)/medial (7) palmar process height, thickness of the sole (8), lateral (9)/medial (10) hoof wall thickness, heel to plumbline (11), toe to plumbline (12), distal interphalangeal joint-to-ground distance (13). Detailed explanations on the 13 hoof measures are provided in Table 2.

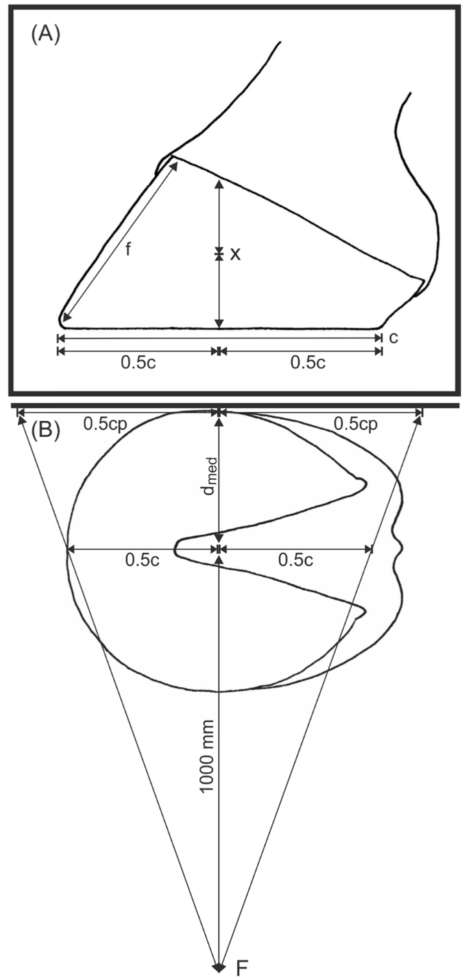

FIGURE 3 | Simplified calculation of the correction factor for hoof measurements in radiographs recorded in lateromedial projection. (A) Hoof position in front of the X-ray detector (rectangle framed in black) as for lateromedial radiography, lateral view, and (B) solear view (detector = strong black line). The central beam (X) was positioned into the approximate hoof midpoint. Measures with the largest distortion such as dorsal hoof wall length (f) were supposed to be in a distance of 0.5 weight-bearing length (c) from the central beam. The distance of the landmarks for f from the X-ray detector equalled the medial hoof width (d_{med}). The focus of the X-ray generator (F) was positioned 1000 mm from the hoof midpoint (2000 mm for 2-m focus-object distance). The expected projection size of 0.5 c (i.e., 0.5 cp) was calculated using the intercept theorem: 0.5 cp/0.5 c = (1000 mm + d_{med})/1000 mm (insert 2000 mm instead of 1000 for 2-m focus-object distance). Measures *c* and d_{med} were taken as recorded from computed tomography images. The factor necessary to calculate the expected real size of all measures from their projection size was 0.5 c/0.5 cp.

necessary. CT measurements based on bony landmarks alone or bony and soft tissue landmarks combined were performed using a bone window histogram setting (window width 3100 HU, window level + 500 HU), measurements with exclusively soft tissue landmarks in a soft tissue window setting (window width 280 HU, window level + 50 HU).

2.3 | Volume Rendering

In order to perform measurements aided by three-dimensional (3D) models of the hoof and its bones, reconstructions of the hooves and the digital bones were generated from the CT datasets using a workstation equipped with the 3D image processing and analysis software Amira 2019.1 (FEI SAS, ThermoFisher Scientific, Waltham, Massachusetts, USA).

Volumes were filtered with a 3D bilateral filter and a 3D Gaussian filter to increase the signal-to-noise ratio. After threshold segmentation of the bones (threshold = 450 HU), the Amira volume segmentation tool 'Volume edit' was used to edit the phalanges, the sesamoid bones and the distal end of the metacarpal bone. Manual correction was necessary whenever the space between two bones at the joint surfaces was too narrow to allow automated threshold-based separation of the bones. To visualise the hoof capsule, a second model was displayed, and the Hounsfield units were adjusted so that the hoof capsule was visible but appeared translucent.

Hoof measures were collected from arbitrarily oriented sections and maximum intensity projections. Orientation was aided by the 3D rendered digital bones as well as directly by the rendered 3D hoof models after identification of the necessary landmarks using auxiliary levels and points within the freely rotatable models.

2.4 | Data Correction and Analysis

For calculation of the projection magnification correction factor for radiographs, one has to consider the distance between landmarks of the measure and central beam, the distance between landmarks and X-ray detector and the relative position of the landmarks to each other as well as the tilt of the central beam in order to include magnification as well as parallax. This was not practicable in our study since the position and tilt of the central beam were not defined with sufficient mathematical precision.

Instead, the magnification factors for Xray 1 m and Xray 2 m were calculated for each individual hoof, as described in Figure 3 using the intercept theorem. The respective correction factors were then applied to all measuring results generated from 1 and 2 m FOD radiographs (Xray 1 m corr and Xray 2 m corr).

For visual comparison, a set of representative measures of the six individual hooves was depicted graphically. Bland–Altman plots (Bland and Altman 1986) were used to show the relation between CTw and each other method to assess whether one method generally gives smaller or larger results than the other and whether small or large values are more affected (Giavarina 2015). To evaluate the agreement between the workflows, the Spearman rank correlation was calculated using SPSS (version 29.0.2.0; IBM, Armonk, New York, USA). For the purpose of this study, each hoof measure assessed by the different workflows has been regarded as an independent variable, although measurements collected from one hoof are, in fact, influenced by each other.

3 | Results

The hoof measures selected for analysis represented small and large measures with landmarks situated near to and distant from the central beam. This allowed for obtaining an overview of possible factors leading to differences between the workflows. Twelve of the thirteen selected measures could be collected by all methods. The dorsal hoof wall length could not be recorded from Xray Sim due to the missing radio-opaque marking and the lack of image contrast between skin and hoof capsule in the average intensity projection image. The dorsal hoof wall length was nevertheless included in the primary analysis as a clinically important large measure at the outer hoof edge, that is, distant from the central beam. Figure 4 provides an overview of the appearance of the hoof with the used imaging techniques.

A first comparison of all hoof measures recorded from Xray 1 m and CTw has confirmed our findings from the previous study. CTw produced constantly lower values than Xray 1 m, with only a few exceptions. Increasing the FOD to 2 m reduced the differences between Xray and CTw data but did not eliminate them completely. Figure 5 shows the comparison for four representative measures—small and large and distant from and near to the central beam. The complete data set can be found in Appendix S1.

Magnification in radiographs compared to CTw ranged between 0.0% and 39.8% for 1-m FOD and 0.0% and 31.77% for 2-m FOD for the individual measures. Measures that produced occasionally (but not always) paradoxically larger CTw values included medial and lateral palmar process height (5 of 12 values for Xray 1 m and 8 of 12 for Xray 2 m), medial and lateral hoof wall thickness (3 of 12 and 9 of 12), dorsal hoof wall length (1 of 6 and 6 of 6), weight-bearing length (3 of 6 and 4 of 6), heel to plumb line (3 of 6 and 3 of 6) and toe to plumbline (3 of 6 for Xray 2 m only) (Appendix S1).

In a second step, we attempted to approximate the supposedly correct CTw values by mathematical correction using individually calculated factors for radiographs (Xray 1 m corr and Xray 2 m corr), by simulating orthogonal radiographs from CT data sets (Xray Sim)

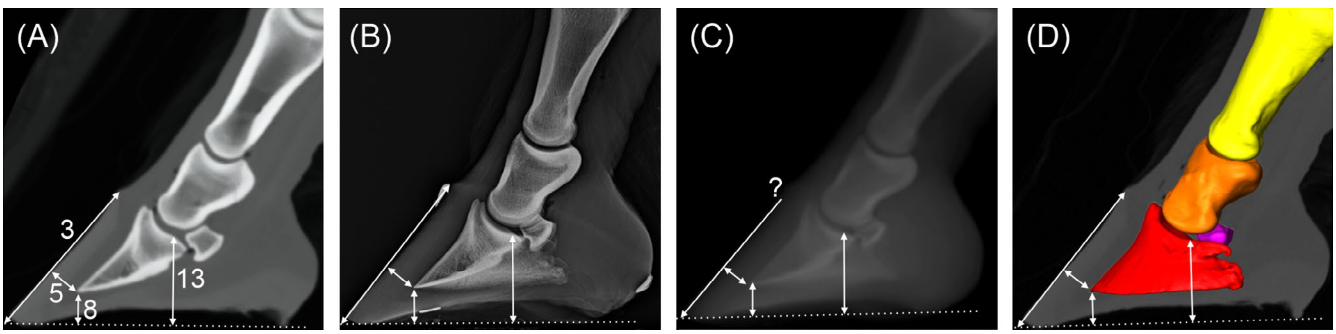

FIGURE 4 | Imaging techniques visualising the equine hoof—appearance of the slides as used for measuring: (A) Computed tomography (CT), 3-mm slab (average intensity projection) reformatted in sagittal plane in the limb axis as defined by anatomical landmarks; (B) Radiograph with radio-opaque markers, focus-object distance 1 m; (C) 120-mm slab reconstructed from CT data set in average intensity projection to simulate an orthogonally projected radiograph in lateromedial projection; (D) three-dimensional reconstruction of digital bones and hoof, orthogonal projection based on the CT dataset, built in the Amira software. Lines with arrows demonstrate four representative hoof measures: (3) dorsal hoof wall length (large measure distant to central beam), (5) distal dorsal hoof wall thickness (small measure distant to central beam), (8) sole thickness (small measure nearer to central beam than 5) and (13) distal interphalangeal joint-to-ground distance (large measure near central beam). For the description of the measures, refer to the numbers in Table 2. Dotted lines represent auxiliary lines based on anatomical landmarks. (?), proximal landmark of 3 not identifiable due to lacking demarcation between hoof horn and skin (radio-opaque markers cannot be used in CT).

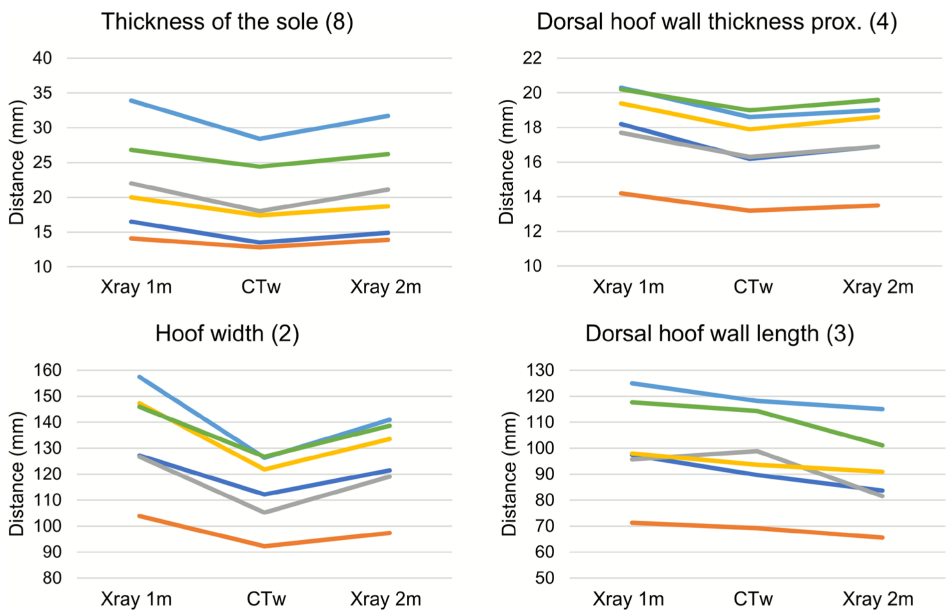

FIGURE 5 | Comparison of values for representative hoof measures recorded from radiographs with 1 m focus-object distance (FOD) (Xray 1 m), from computed tomography images in planes defined based on anatomical landmarks (CTw) and from radiographs with 2-m FOD (Xray 2 m). Increasing FOD reduced the difference to CTw values but did not eliminate it. Each analysed hoof is represented by one coloured line ($n=6$). The numbers in the chart titles refer to the numbers of measures in Table 2 and Figure 2.

and by 3D reconstruction of the hooves and measuring aided by the 3D models (AMIRA) (Appendix S1). Xray Sim values were slightly but nearly constantly lower than CTw values. Similarly, AMIRA values were mostly lower than the CTw values. Exceptions were weight-bearing length, hoof width, sole thickness and a few individual cases for the other measures (Figure 6, Appendix S1).

Bland–Altman plots (comparison with CTw Figure 7, all other comparisons see Appendix S2) were used to evaluate the agreement between the workflows and to verify any systematic bias. Dorsal hoof wall length was excluded due to the incomplete data set. When comparing all analysed workflows against each other, the mean of differences ranged around zero between −3.59 and 5.10 mm (CTw vs. Xray 1 m and Xray 1 m vs. AMIRA, respectively) (Appendix S2). The best match was found between CTw and Xray 2 m corr. Xray Sim and AMIRA produced nearly identical values, too. Measuring in radiographs without mathematical correction yielded systematically higher AMIRA lower values than all other methods (even if they were near to Xray Sim). The corresponding means of differences ranged between 1.29–5.10 mm or 2.83%–12.01% for Xray and 0.28–5.10 mm or 2.18%–12.01% for AMIRA.

An increase in the variability of the differences with increasing magnitude of the measured value could be observed when expressed in absolute numbers for nearly all method comparisons, that is, large values were more different from each other than small values when collected with two different methods. This was confirmed by outliers situated outside the agreement limits (mean of differences ± (1.96 × standard deviation of differences)): 31 and 29 outliers (total number of compared differences = 1284) were found for hoof width and weight-bearing length, respectively, the two largest analysed hoof measures. Fewer values situated outside the agreement limits were found for heel to plumbline (16), toe to plumbline (6), palmar process height (2) and distal interphalangeal joint-to-ground distance (1). The percentage differences between the methods (Appendix S2) presented a different picture: 30 values outside the agreement limits were detected for heel to plumbline alone, with deviations of approximately 30% from the mean of differences. Other measures with outliers were sole thickness (18 values outside agreement limit), medial and lateral palmar process height (15), hoof wall thickness (7) and toe to plumbline (6).

The correlation between the analysed methods was high and highly significant, despite the discrepancies and variability of the absolute values (Table 3).

4 | Discussion

Collection of hoof measures using various imaging techniques and methods of data acquisition did not produce fully equivalent results. As expected, projection magnification in radiographs resulted in larger values when compared to CTw, similar to a study on human bones by Stevens (1989). Interestingly, discrepancies between Xray and CTw values affected the measurement of structures both near and distant from the central beam. For some measures, CTw values were larger than Xray values, which calls for a separate explanation.

Palmar process height and medial/lateral hoof wall thickness were collected from radiographs in dorsopalmar projection, where correct positioning was difficult. Medio-lateral tilting could not be avoided completely, resulting in possible parallax distortion. Moreover, identification of the widest part of the hoof by scrolling through a series of CT images might have introduced a further source of error. Another factor to be considered is the fact that radiographs are usually taken from loaded digits, whereas CT series are usually recorded from unloaded limbs.

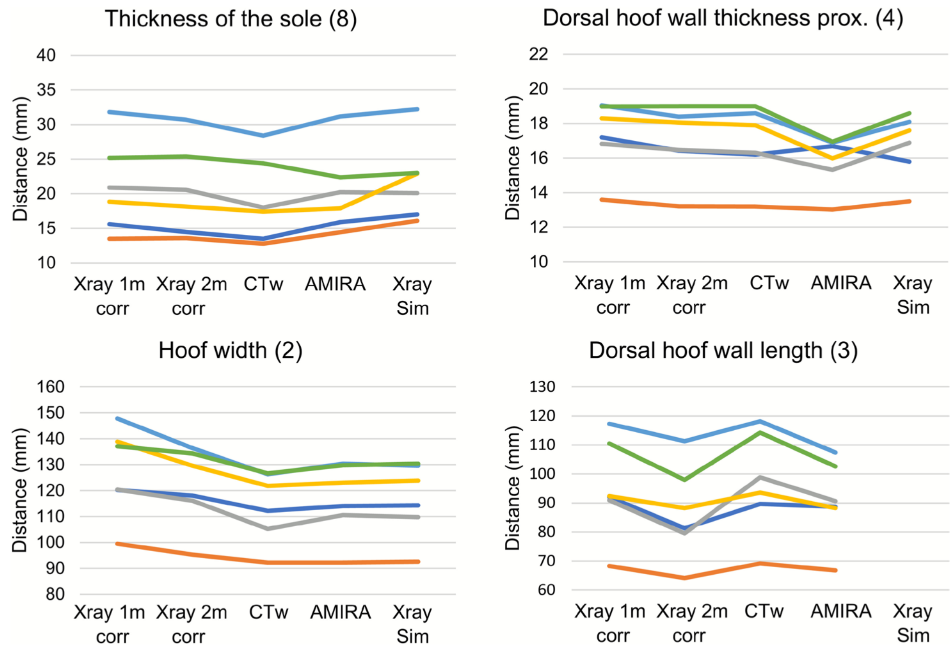

FIGURE 6 | Comparison of mathematically corrected values for representative hoof measures recorded from radiographs with 1 m focus-object distance (FOD) (Xray 1 m corr) and 2 m FOD (Xray 2 m corr), from computed tomography images in planes defined based on anatomical landmarks (CTw), from CT images aided by three-dimensional models (AMIRA), and from simulated radiographs based on the CT dataset (Xray Sim). Mathematical correction often, but not always, led to an approximation of Xray to CTw values. CTw, AMIRA, and Xray Sim data differed from each other, although they were based on the same data set. Each analysed hoof is represented by one coloured line ($n = 6$). The numbers in the chart titles refer to the numbers of measures in Table 2 and Figure 2.

Loading of equine digits leads to heel expansion (Brunsting et al. 2019), resulting in a downwards movement of the palmar processes of the coffin bone and increased hoof capsule inclination (Burn and Brockington 2001; see also Goulet et al. 2015). This shifts the landmarks and potentially enlarges the parallax effect. A similar situation has been noted by Grundmann et al. (2015), who compared hoof measures collected from radiographs and MRI images. However, in our study we expect the influence of hoof mechanics on the measurements to be very small or absent, since the limb was placed in a vertical position supporting its own weight, but no additional loading was applied. Thus, the load of the limb was considerably lower than the weight of a horse. Further research, for example, by comparing radiographs of loaded and unloaded limbs of the same animal, might clarify the influence of load on hoof measures.

Weight-bearing length and heel to plumb line both relied on the identification of the most palmar contact point of the hoof with the ground. In radiographs, this landmark could be identified easily. In CT images, it had to be found using auxiliary lines, since it is not present in the axial plane of the hoof. Erroneous identification of this point might have led to the observed inconsistencies between Xray and CTw values. For heel and toe to plumbline, the different angulation of the distal interphalangeal joint due to the presence or absence of the simulated load did possibly also lead to (small) differences in landmark definition. These two measures produced generally the highest variabilities, as shown by the largest percentage deviations from the mean of differences (Appendix S2).

We attempted to approximate CTw values by using individual correction factors for each hoof to adjust the Xray values, since arbitrary factors (e.g., radiographic magnification = 15%) are known to yield unsatisfactory results (Stevens 1989). A better solution would be to calculate the factor for each measure individually, but this was not possible, since, as usual for standard hoof radiography, the precise position of the central beam had not been recorded. The hoof-specific correction factor should, however, cover the maximally possible projection distortion for landmarks most distant from the central beam, in awareness that this might lead to overcorrection of the other measures. Parallax effects, which are discussed to be a source of imprecisions (Sanfridsson et al. 1998; Spolyar et al. 1993; Stevens 1989; Wells et al. 1991), were not covered in this simple model. Placing an object of known size at the level of a structure of interest before radiography would enable the calculation of a more precise correction factor, but even this does not account for the distortion of structures distant to the object.

Mathematical correction of radiography data (cf. Wechselberg and Wessely 1973) achieved the desired result for some measures both distant from and near to the central beam. Other measures, for example, dorsal hoof wall length, were overcorrected, although their landmarks were as distant from the central beam as, for example, those for the correctly adjusted dorsal hoof wall thickness. Overcorrection occurred in measures that were already larger in CTw than in Xray before correction (Figure 6, Appendix S1).

Simulation of orthogonally projected radiographs from CT data sets has been used successfully for quantification for research purposes (Kau et al. 2020) and diagnosis (e.g., Carey et al. 2021; Rosskopf et al. 2020), in situations where identification of structures was easier in images resembling radiographs than in thin

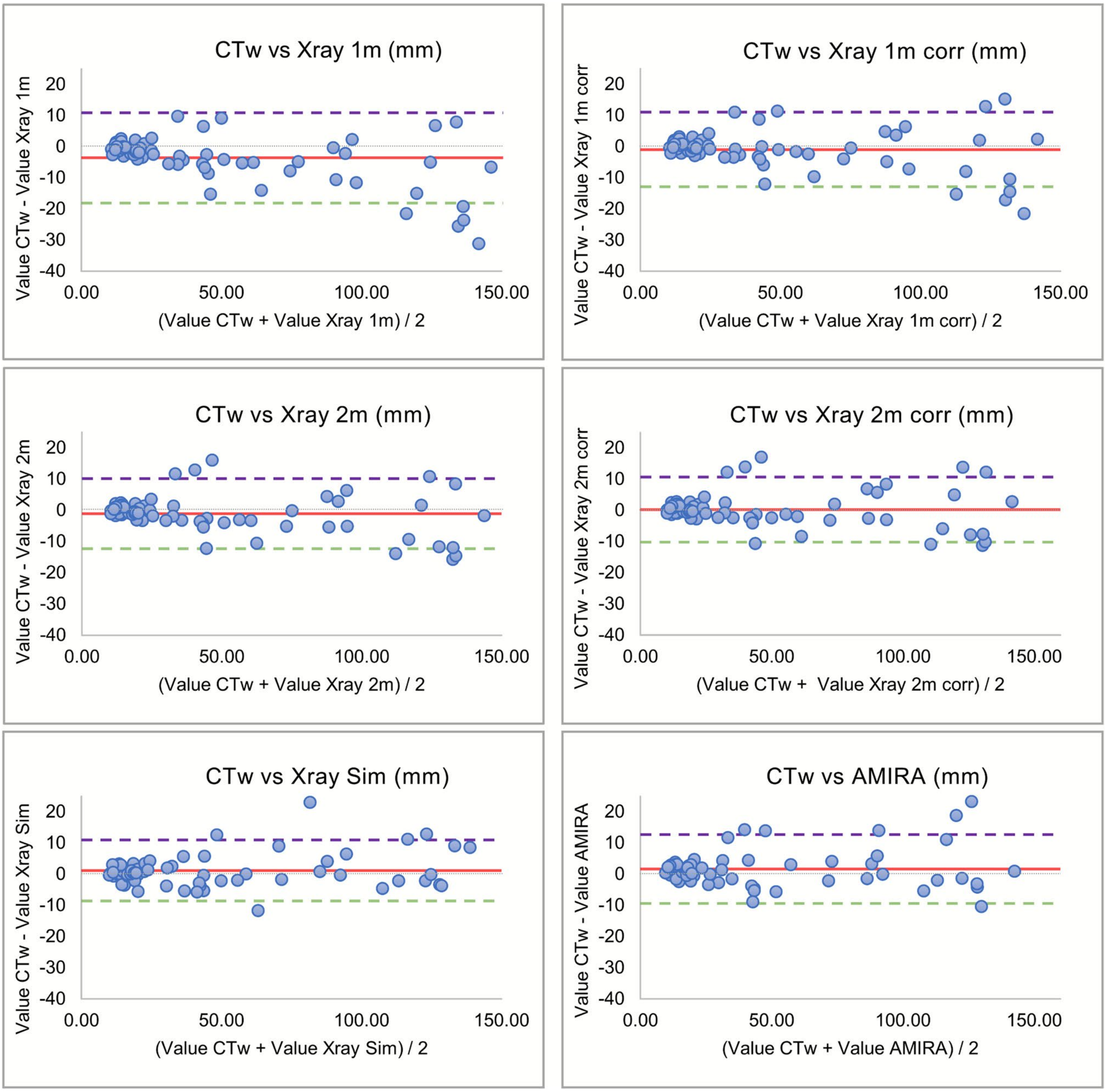

FIGURE 7 | Bland–Altman plots showing the agreement between values for representative hoof measures ($n=72$) recorded using different techniques in comparison with values recorded from computed tomography images in planes defined based on anatomical landmarks (CTw): Xray 1 m and Xray 2 m, measuring in hoof radiographs with 1 m and 2 m focus-object distance without or with mathematical correction (corr); AMIRA, measuring in CT images aided by three dimensional models; and Xray Sim, measuring in simulated radiographs based on the CT dataset. Y-axes show the difference (method 1—method 2), X-axes the mean of measured values ((method 1+ method 2)/2) in mm. The mean of differences was markedly below 0 for CT vs. Xray 1 m (−3.59 mm = −6.19%), demonstrating the systematically higher Xray 1 m values compared to CT values. Middle and large hoof measures showed higher (absolute) deviations. Red line, mean of differences; grey dotted line, line of equality; dashed lines, limits of agreements (mean of differences ±1.96 × standard deviation). Bland–Altman plots of all other method comparisons see Appendix S2.

CT slices. We tested this approach to distinguish projection magnification and parallax effects in radiographs from other possible sources of variance. The discrepancies observed in our study had also been noted by Sun and Jansen (2019) when comparing measuring results from thin slices, thick slabs and volume-rendered models of the same CT data. Such findings are not easy to explain because the measuring workflows draw from the same data set. In our case, smaller Xray Sim values may derive from lower edge contrast in average projections from 120-mm thick slabs, which complicates the exact definition of boundaries, for example, the boundary of a bone embedded in soft tissue.

Similar to Xray Sim, our AMIRA values were often smaller than CTw values, the interpretation of which is even more intricate because both were collected in the same way. The 3D model guided orientation of the virtual CT images allowed potentially a more correct landmark identification, which may be one explanation for the smaller AMIRA values. An alternative

TABLE 3 | Spearman rank correlation coefficient (ρ) for each pairwise combination of measuring workflows. All correlations significant at $p < 0.01$.

	CTw[a]		Xray 1 m[a]		Xay 2 m[a]		Xray Sim[a]		Xray 1 m corr[a]		Xray 2 m corr[a]	
	ρ	CI	ρ	CI	ρ	CI	ρ	CI	ρ	CI	ρ	CI
Xray 1 m[a]	0.984	0.975–0.990										
Xray 2 m[a]	0.987	0.979–0.992	0.997	0.994–0.998								
Xray Sim[a]	0.979	0.966–0.987	0.991	0.985–0.994	0.992	0.987–0.995						
Xray 1 m corr[a]	0.983	0.973–0.990	0.999	0.998–0.999	(0.996)	(0.993–0.997)	0.991	0.985–0.994				
Xray 2 m corr[a]	0.985	0.976–0.991	(0.999)	(0.996–0.999)	0.998	0.997–0.999	0.993	0.988–0.996	(0.997)	(0.995–0.998)		
AMIRA[a]	0.983	0.972–0.989	0.992	0.988–0.995	0.993	0.988–0.996	0.991	0.986–0.995	0.992	0.986–0.995	0.994	0.991–0.997

Abbreviation: CI, 95% confidence intervals.
[a]Xray 1 m and Xray 2 m, measuring in hoof radiographs with 1 m and 2 m focus-object distance without or with mathematical correction (corr); CTw, values recorded from computed tomography images in planes defined based on anatomical landmarks; AMIRA, values recorded from CT images aided by three dimensional models; and Xray Sim, measuring in simulated radiographs based on the CT dataset. Values in parentheses for comparison only, no objective background.

explanation lies in the thickness of the virtual CT images generated using the JiveX software (3-mm slices), which potentially produces slightly higher measuring results compared to measuring in a single virtual CT image ('thickness' smaller or equal to voxel size) as conducted in the AMIRA workflow.

Another source for error could have been in the used contrast settings. The influence of the chosen window parameters on CT measurements is well known (see e.g., the different measuring errors for hard and soft tissue in Cavalcanti et al. 2004). To guarantee repeatable results, the use of dedicated windows for the respective question or even the generation of advanced 'all-in-one' CT images is encouraged (Cebula et al. 2017; Snoeckx et al. 2019). Unfortunately, to our knowledge, optimised bone and soft tissue window settings for hoof analysis tested for performance and approved by the scientific community are not yet available.

Despite the absolute differences between the results of the analysed methods, they showed a very high correlation. High absolute deviations could be detected for those individual measures for which it was most difficult to determine the landmarks (heel to plumbline). In these cases, differences between measuring workflows might rather be a result of identifying and measuring entirely different structures than due to technical reasons such as projection magnification or contrast settings. Whether absolute differences are to be considered too large for comparison of values collected by different workflows depends on the biological question. If in doubt, comparison of ratios between measures might be the better option (Goulet et al. 2015; Grundmann et al. 2015).

4.1 | Summary and Practical Remarks

Increasing FOD when generating radiographs decreases projection magnification (and parallax effects). However, the practicability of this approach is limited due to the reduction in detector dose and the resulting need for higher mAs values, which may exceed the technical limits of the X-ray machine. Even simple mathematical correction approximates Xray values to CTw values.

Measuring in CT images does not necessarily produce 'more correct' values than radiography. Depending on landmark definition, measures with the same name might measure something different (e.g., weight-bearing length of the hoof). The preferred technique should be defined based on the biological question (e.g., for weight-bearing length, data from radiographs probably provide more reliable information on the loaded part of the hoof).

Landmark definition is crucial, regardless of the chosen method. Measures with landmarks in both hard and soft tissues can be difficult to identify. For radiography, radio-opaque markers should be used. Measures requiring reconstruction and auxiliary lines for landmark definition seem to produce more inconsistent results.

High correlation between values collected by different methods does not mean that the absolute measures will be the same. If in doubt, analyse relations between measures rather than absolute values. This is especially relevant when comparing different publications or measures collected by different methods.

Author Contributions

L.S.: conceptualisation, data curation, formal analysis, funding acquisition, investigation, methodology, resources, visualisation, writing – original draft, writing – review and editing. E.L.: methodology, resources, supervision, visualisation, writing – review and editing. S.H.:

methodology, resources, supervision, visualisation, writing – review and editing. K.W.: conceptualisation, data curation, formal analysis, project administration, supervision, visualisation, writing – original draft, writing – review and editing.

Acknowledgements

We would like to thank Dr. Katrin Schieder and Bibiane Pollak (both Diagnostic Imaging—Clinical Center of Small Animals, Clinical Department for Small Animals and Horses, University of Veterinary Medicine Vienna, Austria) for their great technical help in the creation of the radiographs and CT data sets. This study was supported by the Hochschuljubiläumsfonds of City Vienna [H-291437/2019]. This research was supported using resources of the VetCore Facility (VetImaging) of the University of Veterinary Medicine Vienna. Open Access funding provided by Veterinarmedizinische Universitat Wien/KEMÖ.

Funding

This study was supported by the Hochschuljubiläumsfonds of City Vienna [H-291437/2019].

Conflicts of Interest

The authors declare no conflicts of interest.

Data Availability Statement

All original data (measuring results) used for this study are provided in Appendix S1.

References

Bland, J. M., and D. G. Altman. 1986. "Statistical Methods for Assessing Agreement Between Two Methods of Clinical Measurement." *Lancet* 327, no. 8476: 307–310. https://doi.org/10.1016/S0140-6736(86)90837-8.

Brunsting, J., M. Dumoulin, M. Oosterlinck, M. Haspeslagh, L. Lefère, and F. Pille. 2019. "Can the Hoof Be Shod Without Limiting the Heel Movement? A Comparative Study Between Barefoot, Shoeing With Conventional Shoes and a Split-Toe Shoe." *Veterinary Journal* 246: 7–11. https://doi.org/10.1016/j.tvjl.2019.01.012.

Buckle, C. E., V. Udawatta, and C. M. Straus. 2013. "Now You See It, Now You Don't: Visual Illusions in Radiology." *Radiographics* 33, no. 7: 2087–2102. https://doi.org/10.1148/rg.337125204.

Burn, J. F., and C. Brockington. 2001. "Quantification of Hoof Deformation Using Optical Motion Capture." *Equine Veterinary Journal* 33, no. S33: 50–53. https://doi.org/10.1111/j.2042-3306.2001.tb05358.x.

Carey, S., S. Kandel, C. Farrell, et al. 2021. "Comparison of Conventional Chest X Ray With a Novel Projection Technique for Ultra-Low Dose CT." *Medical Physics* 48, no. 6: 2809–2815. https://doi.org/10.1002/mp.14142.

Cavalcanti, M. G. P., S. S. Rocha, and M. W. Vannier. 2004. "Craniofacial Measurements Based on 3D-CT Volume Rendering: Implications for Clinical Applications." *Dento Maxillo Facial Radiology* 33, no. 3: 170–176. https://doi.org/10.1259/dmfr/13603271.

Cebula, M., M. D. Nowak, and S. Modlińska. 2017. "Impact of Window Computed Tomography (CT) Parameters on Measurement of Inflammatory Changes in Paranasal Sinuses." *Polish Journal of Radiology* 82: 567–570. https://doi.org/10.12659/PJR.901939.

Fatemitabar, S. A., and A. Nikgoo. 2010. "Multichannel Computed Tomography Versus Cone-Beam Computed Tomography: Linear Accuracy of In Vitro Measurements of the Maxilla for Implant Placement." *International Journal of Oral & Maxillofacial Implants* 25, no. 3: 499–505.

Gaspoz, F., P. Monnin, D. Petter, J. Plé, and S. Ding. 2015. "Precision and Accuracy of Measurements on CT Scout View." *Journal of Medical Imaging and Radiation Sciences* 46, no. 3: 309–316. https://doi.org/10.1016/j.jmir.2015.06.006.

Giavarina, D. 2015. "Understanding Bland Altman Analysis." *Biochemia Medica* 25, no. 2: 141–151. https://doi.org/10.11613/BM.2015.015.

Goulet, C., J. Olive, Y. Rossier, and G. Beauchamp. 2015. "Radiographic and Anatomic Characteristics of Dorsal Hoof Wall Layers in Nonlaminitic Horses." *Veterinary Radiology & Ultrasound* 56, no. 6: 589–594. https://doi.org/10.1111/vru.12280.

Grundmann, I. N. M., W. T. Drost, L. J. Zekas, et al. 2015. "Quantitative Assessment of the Equine Hoof Using Digital Radiography and Magnetic Resonance Imaging." *Equine Veterinary Journal* 47, no. 5: 542–547. https://doi.org/10.1111/evj.12340.

Kau, S., K. Failing, and C. Staszyk. 2020. "Computed Tomography (CT)-Assisted 3D Cephalometry in Horses: Interincisal Angulation of Clinical Crowns." *Frontiers in Veterinary Science* 7: 434. https://doi.org/10.3389/fvets.2020.00434.

Kruth, J. P., M. Bartscher, S. Carmignato, R. Schmitt, L. De Chiffre, and A. Weckenmann. 2011. "Computed Tomography for Dimensional Metrology." *CIRP Annals - Manufacturing Technology* 60, no. 2: 821–842. https://doi.org/10.1016/j.cirp.2011.05.006.

Kumar, V., J. B. Ludlow, A. Mol, and L. Cevidanes. 2007. "Comparison of Conventional and Cone Beam CT Synthesized Cephalograms." *Dento Maxillo Facial Radiology* 36, no. 5: 263–269. https://doi.org/10.1259/dmfr/98032356.

Mozzo, P., C. Procacci, A. Tacconi, P. Tinazzi Martini, and I. A. Bergamo Andreis. 1998. "A New Volumetric CT Machine for Dental Imaging Based on the Cone-Beam Technique: Preliminary Results." *European Radiology* 8, no. 9: 1558–1564. https://doi.org/10.1007/s003300050586.

Nilsson, T., J. Ahlqvist, M. Johansson, and A. Isberg. 2004. "Virtual Reality for Simulation of Radiographic Projections: Validation of Projection Geometry." *Dento Maxillo Facial Radiology* 33, no. 1: 44–50. https://doi.org/10.1259/dmfr/22722586.

Rosskopf, J., C. Kloth, J. Dreyhaupt, M. Braun, B. L. Schmitz, and T. Graeter. 2020. "Thin Slices and Maximum Intensity Projection Reconstructions Increase Sensitivity to Hyperdense Middle Cerebral Artery Sign in Acute Ischemic Stroke." *Cerebrovascular Diseases* 49, no. 4: 437–441. https://doi.org/10.1159/000509378.

Sanfridsson, J., G. Svahn, L. Ryd, T. L. Ahl, P. Sundén, and K. Jonsson. 1998. "Assessment of Image Post-Processing and of Measuring Assistance Tools in Computed Radiography: Evaluation of the Weight-Bearing Knee." *Acta Radiologica* 39, no. 6: 642–648. https://doi.org/10.3109/02841859809175490.

Sellke, L., B. Patan-Zugaj, E. Ludewig, R. Cimrman, and K. Witter. 2023. "Comparison of Six Different Methods for Measuring the Equine Hoof and Recording of Its Three-Dimensional Conformation." *Journal of Equine Veterinary Science* 121: 104195. https://doi.org/10.1016/j.jevs.2022.104195.

Sellke, L., B. Patan-Zugaj, and K. Witter. 2020. "Nomenclature of Equine Hoof Measurements—A Systematic Literature Review." *Pferdeheilkunde* 36, no. 3: 238–251. https://doi.org/10.21836/PEM20200306.

Snoeckx, A., J. Cant, C. Franck, et al. 2019. "Lesion Measurement on a Combined All-In-One Window for Chest CT: Effect on Intra- and Interobserver Variability." *Cancer Imaging* 19: 78. https://doi.org/10.1186/s40644-019-0262-0.

Spolyar, J. L., W. Vasileff, R. B. MacIntosh, and B. Rune. 1993. "Image Corrected Cephalometric Analysis (ICCA): Design and Evaluation." *Cleft Palate-Craniofacial Journal* 30, no. 6: 528–541. https://doi.org/10.1597/1545-1569_1993_030_0528_iccaid_2.3.co_2.

Stevens, P. M. 1989. "Radiographic Distortion of Bones: A Marker Study." *Orthopedics* 12, no. 11: 1457–1463. https://doi.org/10.3928/0147-7447-19891101-11.

Sun, Z., and S. Jansen. 2019. "Personalized 3D Printed Coronary Models in Coronary Stenting." *Quantitative Imaging in Medicine and Surgery* 9, no. 8: 1356–1367. https://doi.org/10.21037/qims.2019.06.21.

Tjernström, B., O. Jakobsson, P. Pech, and L. Rehnberg. 1996. "Reliability of Radiological Measurements of the Distraction Gap During Leg Lengthening." *Acta Radiologica* 37, no. 2: 162–165. https://doi.org/10.3109/02841859609173437.

Vasconcellos, A. C. R. S., A. D. S. Maciel, C. M. F. Rubira, I. R. F. Rubira-Bullen, and V. A. Sarmento. 2015. "Accuracy of Linear Measurement in Computed Tomography: A Systematic Review." *International Journal of Enhanced Research in Science Technology & Engineering* 4, no. 2: 79–88.

Wechselberg, K., and J. Wessely. 1973. "Planimetrische Methode an Röntgenbildern kindlicher Hirnschädel mit Normwerten für das Kindesalter." *Zeitschrift für Kinderheilkunde* 114, no. 1: 39–53. https://doi.org/10.1007/BF00446116.

Wells, T. R., B. H. Landing, and E. M. Padua. 1991. "The Question of Parallax-Effect on Radiographic Assessment of Short Trachea in Infants and Children." *Pediatric Radiology* 21, no. 7: 490–493. https://doi.org/10.1007/BF02011719.

Supporting Information

Additional supporting information can be found online in the Supporting Information section. **Appendix S1:** Original data and comparison of values collected by different methods for measuring in radiographs and computed tomograms. **Appendix S2:** Bland–Altman plots for evaluation of the agreement between different methods measuring in radiographs and computed tomograms.